SIAM J. APPL. MATH.
Vol. 86, No. 1, pp. 133–159

PRANDTL–BATCHELOR THEORY FOR AN ANNULAR DOMAIN*

SUN-CHUL KIM† AND JUNE-YUB LEE‡

Abstract. The Prandtl–Batchelor theory for steady Navier–Stokes flows at large Reynolds numbers is extended to multiply connected two-dimensional domains. In this study, we investigate incompressible flows in a concentric annulus. A proper mathematical formulation is established, and we derive the corresponding Batchelor–Wood formula for the limiting vorticity. Our analysis reveals that the vorticity is a constant while the angular velocity is a linear combination of r and r^{-1}. Under the perturbation of the outer boundary velocity, we asymptotically calculate the effects of a finite Reynolds number and compare our results with numerical computations. We also examine cases involving the inner and both perturbed boundary velocities. The results show good agreement for small perturbations at large Reynolds numbers, confirming the validity of the theory. Notably, we observe the formation of a weak layer near the unperturbed boundary, where the vorticity is discontinuous while the velocity remains continuous. This discrepancy can be regarded as an intriguing characteristic of the inviscid limit flows. Finally, we discuss potential extensions of our findings for future research.

Key words. vortex flows, boundary layers, annular domain, inviscid limit

MSC codes. 76D05, 76D10, 76D17, 76D30

DOI. 10.1137/25M1751098

1. Introduction.

There are many interesting yet complex singular phenomena in incompressible steady-state Navier–Stokes flows as the Reynolds number R becomes very large. One such example is the boundary layer, for which Prandtl [24] first developed an efficient theory for explanation and analysis. He also proposed a relevant asymptotic behavior for such flows as R increases. Specifically, he found that the vorticity tends to a uniform constant in regions with nested closed streamlines. This property was later rediscovered by Batchelor [2], who studied specific examples and derived a formula for the limiting constant vorticity in the circular domain case.

This is the initial development of the "Prandtl–Batchelor" (PB) theory for incompressible Navier–Stokes flows at large Reynolds numbers. Since then, the theory has been generalized in various directions, such as flows with certain geometric symmetries [6], some three-dimensional flows [3, 27], cylindrical [9] and periodic [21] domains, time-dependent flows [1], and even some geophysical flows [36]. Additionally, there have been numerous applications of the theory to real physical flows [4, 5, 26, 28].

However, focusing on the theoretical aspects of PB theory in two dimensions, we find that most of the results are essentially confined to simply connected regular domains [11, 12, 14]. These include a disk [18] or regions with corners [33]. In such cases, the vorticity can be effectively calculated using a formula given in [2], which was later extended by Wood [35]. This is known as the "Batchelor–Wood" (BW) formula and serves as a starting point for determining the vorticity value. (See also

*Received by the editors April 14, 2025; accepted for publication (in revised form) September 23, 2025; published electronically January 9, 2026.
https://doi.org/10.1137/25M1751098
Funding: The work of the first author was supported by the National Research Foundation of Korea (NRF) funded by the Korea government (MSIT) grant RS-2023-00240538. The work of the second author was supported by the National Research Foundation of Korea (NRF) funded by the Korea government (MSIT) grant RS-2023-00273584.
†Department of Mathematics, Chung-Ang University, Seoul, 06974 Korea (kimsc@cau.ac.kr).
‡Department of Mathematics, Ewha Womans University, Seoul, 03760 Korea (jyllee@ewha.ac.kr).

[16] for an elliptic domain, [32] for discontinuous boundary conditions, and [34] for polygonal domains.) Subsequently, Feynman and Lagerstrom [14] proposed applying this formula to a general two-dimensional domain as a reasonable approximation, which was rigorously studied in recent work [11]. There have been relevant works when the BW formula cannot be expected to be accurate [25, 31]. Nevertheless, all these results pertain to simply connected domains in two dimensions except a very recent work on the existence of PB flows in an annulus [13].

In this paper, we extend the PB theory to general multiply connected domains, using the annulus as a simple and concrete example. We first develop the corresponding theoretical framework for large R and then validate the results through appropriate numerical computations. Specifically, assuming the flow depends only on r, we find that the inviscid limit vorticity is given by a linear function of the logarithm. For the perturbed case with ϵ the perturbation parameter for the boundary velocity, we compute the flow up to the order of $\epsilon^2/\sqrt{R}$, and compare the results with precise numerical data. The comparison shows good agreement between the theoretical predictions and the numerical results. Additionally, we consider the case where both the inner and outer boundary velocities are perturbed, providing a proper interpretation of the obtained result.

The contents of the paper are as follows. In section 2, we develop an analogous PB theory for an annular domain under certain conditions. The corresponding BW formula is derived in section 3. In section 4, we compute the second-order expansion of the flow in R under a perturbation of the boundary velocity, using an asymptotic matching method. The numerical method used for highly accurate computations is explained in section 5. In section 6, the numerical results are presented and compared with the asymptotic calculations. Finally, we conclude with remarks on the case of general multiply connected domains in section 7. The details of the asymptotic calculations are provided in the appendix at the end of the paper.

2. PB theory for an annulus. The two-dimensional steady incompressible Navier–Stokes equations for a flow velocity $\mathbf{u} = (u, v, 0)$ are

$$\mathbf{u} \cdot \nabla \mathbf{u} + \nabla p = R^{-1} \nabla^2 \mathbf{u}, \quad \nabla \cdot \mathbf{u} = 0, \tag{2.1}$$

where p is the pressure and R is the Reynolds number. We consider the flow in an annular domain

$$D = \{(r, \theta) : r_1 < r < r_2,\ 0 \le \theta < 2\pi\}$$

for some positive $r_1 < r_2$ with given boundary velocity

$$u_r|_{r_1} = u_r|_{r_2} = 0, \quad u_\theta|_{r_1} = q_1, \quad u_\theta|_{r_2} = q_2,$$

respectively. Here u_r, u_θ denote the r, θ components of the velocity, and we consider a boundary driven flow inside an annulus in this paper. For the scaling, we take $r_2 = 1$ in section 4, but further simplification is not possible as q_1, q_2 are not constants in general.

From the incompressibility, we introduce the stream function $\psi(r, \theta)$ by

$$\frac{1}{r}\frac{\partial \psi}{\partial \theta} = u_r, \quad \frac{\partial \psi}{\partial r} = -u_\theta$$

as usual. Also, defining the vorticity $\omega = -\nabla^2 \psi$, we obtain

$$\mathbf{u} \cdot \nabla \omega = R^{-1} \nabla^2 \omega. \tag{2.2}$$

Thus writing the inviscid limit vorticity $\omega_0 = \lim_{R\to\infty}\omega$, we find that for the Euler flow, i.e., $R\to\infty$,

$$\mathbf{u}\cdot\nabla\omega_0 = 0. \tag{2.3}$$

This indicates that ω_0 is a function of ψ alone.

For the Navier–Stokes flow inside the annulus D, we take any two different streamlines $\psi = c_1$, $\psi = c_2$ for $c_1 \neq c_2$ to integrate (2.2) on an annulus $c_1 \le \psi \le c_2$. Applying Green's theorem, we obtain

$$\oint_{\psi=c_1}\left(u_n\omega - \frac{1}{R}\frac{\partial\omega}{\partial n}\right)\,ds = \oint_{\psi=c_2}\left(u_n\omega - \frac{1}{R}\frac{\partial\omega}{\partial n}\right)\,ds, \tag{2.4}$$

where u_n is the normal component of u, $\partial/\partial n$ is the normal derivative, and s is the arc length. Since $u_n = 0$ on a streamline, (2.4) reduces to

$$\frac{1}{R}\oint_{\psi=c_1}\frac{\partial\omega}{\partial n}\,ds = \frac{1}{R}\oint_{\psi=c_2}\frac{\partial\omega}{\partial n}\,ds. \tag{2.5}$$

Here we may drop $1/R$ from both sides and send $R\to\infty$. Using $\omega_0 = \omega_0(\psi)$ from (2.3) in the limit, we find

$$\gamma(c_1)\omega_0'(c_1) = \gamma(c_2)\omega_0'(c_2), \tag{2.6}$$

where $\gamma(\psi)$ is the circulation integral along the streamline $\psi = c_1$,

$$\gamma(c_1) = \oint_{\psi=c_1} q\,ds, \quad q^2 = u_r^2 + u_\theta^2. \tag{2.7}$$

Therefore we obtain the following identity for any closed $\psi(x,y) = c$ inside D,

$$\gamma(c)\omega_0'(c) = K = \text{constant}, \tag{2.8}$$

which is the corresponding result of PB theory for an annulus.

Historically, the result was first obtained by Prandtl [24] for a steady region of closed streamlines with no hole inside. In this case, using the same argument, we deduce $K = 0$. Thus the limiting vorticity is shown to be a uniform constant throughout the region enclosed by a closed streamline $\psi = c$. Later, Batchelor independently confirmed this result and went on to calculate the exact constant vorticity ω_0 for the case of a concentric circular flow. Below, we derive the analogous extension of this result for the case of an annulus.

3. BW formula for an annulus. Let us proceed further from (2.8) to determine the limiting vorticity (and the flow). Assuming that all streamlines are circular, we have

$$\partial n = \partial r, \quad q = -\frac{d\psi}{dr} = \text{constant} \tag{3.1}$$

on any closed streamline $\psi = c_1$. Thus we simplify (2.8) to

$$\frac{d\omega}{dr} = \frac{K_0}{r}, \tag{3.2}$$

where K_0 is a constant (to be determined). Consequently, ω becomes a nonconstant function of r. Integrating (3.2) on r, we obtain

$$\omega = K_0 \log r + K_1$$

for another constant K_1. This is the main difference from the simply connected domain case where the limit vorticity becomes constant throughout the whole domain. But, for an annulus, we have the vorticity given by a logarithmic linear function of r. Accordingly, there are two unknown constants to be determined from a proper matching of the inviscid limit Euler flow and the viscous flow. For a general domain, it is difficult to find the exact formula for the flow. However, for a concentric annulus, we provide a simple example below.

Additional integration on r yields

$$\psi = Ar^2 \log r + Br^2 + C \log r, \tag{3.3}$$

where $A = -K_0/4$, $B = (K_0 - K_1)/4$, C are constants to be determined. We note here that the boundary values of ψ at $r = r_1$, $r = r_2$ do not completely determine the three constants. This is a well-known property of nonuniqueness of the solution of Navier–Stokes equations in a multiply connected domain. However, in the special case of inviscid limit preserving the single-eddy configuration, we obtain the uniqueness from PB theory and the single valuedness of pressure [22] in section 3.1. This will be explained in detail below. For a rigorous argument, see [13].

For a general boundary speed given along $r = r_1$, $r = r_2$, there generally appear two boundary layers of thickness $O(1/\sqrt{R})$ as $R \to \infty$. Let us denote the corresponding Euler limit speed as q_{e1}, q_{e2} for $r = r_1$, $r = r_2$, respectively. (These are given in the limit of the outer flow away from the boundary layers.)

We first consider the boundary layer formed near the outside boundary. The equations of the boundary layer may be written in coordinates ξ, η, where $\xi = s$ is the arc length and η the distance normal to the boundary measured from the wall toward the interior, times $\sqrt{R}$. Let the corresponding velocity coordinates be u_ξ, u_η, that is, u_η is the component in the direction of the inward normal times $\sqrt{R}$. We also denote q_e as the limit of the inviscid flow velocity as one approaches the boundary; we obtain

$$u_\xi \frac{\partial u_\xi}{\partial \xi} + u_\eta \frac{\partial u_\xi}{\partial \eta} - q_e(\xi) q_e'(\xi) - \frac{\partial^2 u_\xi}{\partial \eta^2} = 0, \quad \frac{\partial u_\xi}{\partial \xi} + \frac{\partial u_\eta}{\partial \eta} = 0. \tag{3.4}$$

These equations hold for $0 \le \xi < 2\pi r_2$, $0 \le \eta < \infty$. We will usually prefer to write (3.4) in terms of von Mises variables $s, \bar{\psi}$, where $s = \xi$, $\bar{\psi} = \sqrt{R}\psi$. Setting $u_\xi = q(s, \bar{\psi})$, we write the boundary layer equation (3.4) in the following form:

$$\frac{\partial q^2}{\partial s} - \frac{dq_e^2}{ds} - q \frac{\partial^2 q^2}{\partial \bar{\psi}^2} = 0. \tag{3.5}$$

We are interested in solving (3.5) for $q(s, \bar{\psi})$ satisfying the conditions

$$q(s + 2\pi r_2, \bar{\psi}) = q(s, \bar{\psi}), \quad q(s, 0) = q_w(s), \quad q(s, \infty) = q_e(s), \tag{3.6}$$

where q_w is the true wall velocity on $r = r_2$.

Here the pressure gradient vanishes identically in the circular domain and (3.5) simplifies into

$$2 \frac{\partial q}{\partial s} - \frac{\partial^2 q^2}{\partial \bar{\psi}^2} = 0. \tag{3.7}$$

Thus, integrating (3.7) for s from 0 to $2\pi r_2$ and making use of (3.6), we obtain

$$\frac{d^2}{d\bar{\psi}^2}\oint_{\bar{\psi}} q^2\ ds = 0,$$

where the integral is over a streamline $\bar{\psi} =$ constant [2]. Assuming that q^2 is bounded for large $\bar{\psi}$ (recall $\bar{\psi} = \sqrt{R}\psi$), we obtain

$$\oint_{\bar{\psi}} q^2\ ds = \text{constant}.$$

Thus, considering similarly for the boundary layer formed inside, we obtain

$$\int_0^{2\pi} q_{e1}^2\, d\theta = \int_0^{2\pi} q_1^2(\theta)\, d\theta, \quad \int_0^{2\pi} q_{e2}^2\, d\theta = \int_0^{2\pi} q_2^2(\theta)\, d\theta, \tag{3.8}$$

where q_{e1}, q_{e2} denote the constant Euler limit speed on the boundary $r = r_1$, $r = r_2$ and q_1, q_2 are the given wall speed on the boundary $r = r_1$, $r = r_2$. These are BW formulas for an annulus, which determine the unknown constants A, B, C if combined with the single valuedness of pressure below and thus the flow completely. Note here that for an eccentric annulus, (3.8) gives only an approximation as the pressure gradient does not identically vanish.

3.1. A condition for single valuedness of pressure. An essential condition for the flow in an annulus is the single-valued property of the pressure. This can be written in many different ways, but usually represented as an integral identity along a closed streamline. (See [15].) Here, for convenience, we adopt the following form of the vorticity integral along a streamline. We begin with the θ component of the stationary Navier–Stokes equations (2.1) in polar form:

$$u_r + \frac{\partial}{\partial\theta}\left(\frac{1}{2}u_\theta^2 + p\right) = \frac{1}{R}\left(\Delta u_\theta - \frac{u_\theta}{r^2} - \frac{2}{r^2}\frac{\partial u_r}{\partial\theta}\right). \tag{3.9}$$

Using $u_r = 0$ on $r = r_1$, we rewrite (3.9) into

$$\frac{u_\theta}{r}\frac{\partial u_\theta}{\partial\theta} + \frac{1}{r}\frac{\partial p}{\partial\theta} = \frac{1}{R}\frac{\partial\omega}{\partial r} \tag{3.10}$$

from the fact $\Delta\mathbf{u} = -\nabla\times\omega$. Since the integral of the left side of (3.10) along the inner boundary must be zero, we obtain

$$\oint_{r=r_1} \frac{\partial\omega}{\partial r} d\theta = 0. \tag{3.11}$$

This condition will be used both in the asymptotic expansion and also in the numerical computation below.

Now, using the condition, we immediately have

$$\omega' = K_0/r = 0,$$

and thus $A = 0$, which implies no log term in the inviscid limit PB flow. Then the boundary condition at two boundary determines the other two constants. Explicitly, we write the system of linear equations

$$2Br_1 + \frac{C}{r_1} = -q_{e1}, \quad 2Br_2 + \frac{C}{r_2} = -q_{e2}$$

to solve and obtain

$$B = \frac{r_2 q_{e2} - r_1 q_{e1}}{2(r_1^2 - r_2^2)}, \quad C = \frac{r_1 r_2 (r_2 q_{e1} - r_1 q_{e2})}{r_1^2 - r_2^2}. \tag{3.12}$$

4. Asymptotic expansion up to second order. We calculate the flow asymptotically by the matched asymptotic expansion method [18]. Putting ϵ, the perturbation parameter for wall data (see below) fixed small enough, we let $R \to \infty$. We shall expand the resulting system of inner and outer expansions in R with respect to ϵ, in order to calculate the viscous corrections to PB theory. Our specific aim is an $O(\epsilon^2/\sqrt{R})$ correction to the inviscid limit vorticity. To simplify the matter, we assume the unperturbed flow depending on r only.

4.1. The principle of transcendental decay of ω to a constant. In order to incorporate the matching technique, we need to investigate the behavior of the vorticity as we approach the outer edge of the boundary layer. In the case of the Blasius flat plate, where the flow outside the boundary layer is uniform and the vorticity vanishes, the vorticity decays to zero transcendentally (usually exponentially; see [30]). Whereas, in the disk flow, a similar principle is found, showing decay to a (possibly nonzero) constant [18].

Now in the present case, the equation for ω_n (the nth order vorticity in the asymptotic expansion; see (4.1) below) becomes too complicated to solve analytically in a closed form. Therefore, we suppose an additional condition that ω_n is a function of r only to make the problem approachable. In fact, we need to suppose $\psi = \psi(r)$, a little stronger condition to proceed hereafter. Physically, this means that we primarily focus on the perturbations of rigid body rotation in this paper. We find that this assumption is reasonable for small perturbations in wall velocity, as confirmed by comparisons with numerical results in the later sections.

Then the vorticity for every order becomes a constant similar to the disk flow case in the following argument. Let us assume that PB theory applies to a concentric annulus D. We also suppose that the vorticity is a function of r only for any order n and is expanded in R near $R = \infty$ of the form

$$\omega(r,R) = \omega_1(r) + A_2(R)\omega_2(r) + \cdots + A_n(R)\omega_n(r) + R_{n+1}(r,R), \tag{4.1}$$

where $A_k(R), k = 1, 2, \ldots$ form an asymptotic sequence with $A_{k+1}(R) = o(A_k(R))$ as $R \to \infty$. Here $R_{n+1}(r,R)$ is the remainder term satisfying $R_{n+1}(r,R) = o(A_n(R))$. Correspondingly the velocity $\mathbf{u}$ is supposed to be expanded by

$$\mathbf{u}(r,R) = \mathbf{u}_1(r) + A_2(R)\mathbf{u}_2(r) + \cdots + A_n(R)\mathbf{u}_n(r) + \widetilde{R_{n+1}}(r,R). \tag{4.2}$$

In order to compute $\omega_n(r)$ we use (2.4) to obtain

$$\oint_{\psi=c_1} \frac{\partial \omega_1}{\partial n}\, ds = \oint_{\psi=c_2} \frac{\partial \omega_1}{\partial n}\, ds, \quad \oint_{\psi=c_1} \frac{\partial \omega_2}{\partial n}\, ds = \oint_{\psi=c_2} \frac{\partial \omega_2}{\partial n}\, ds, \ldots. \tag{4.3}$$

Let us consider the result after substituting (4.1), (4.2) into (2.2). Collecting $O(1)$ terms and applying (4.3), we recover the result $\omega_1(r) = \omega_1 = K_1 \log r + K_2$ for the annulus, where K_1, K_2 are constants. But together with the single-valued condition, it follows that $K_1 = 0$ and $\omega_1 = K_2$. Utilizing this result in (2.2) and considering next order terms, we find $A_2(R) = 1/R$ and obtain the following equation:

$$\mathbf{u}_2 \cdot \nabla \omega_1 + \mathbf{u}_1 \cdot \nabla \omega_2 = \nabla^2 \omega_1. \tag{4.4}$$

Accordingly, as $R \to \infty$, we simplify (4.4) into

$$\mathbf{u}_1 \cdot \nabla \omega_2 = 0$$

which shows that $\omega_2 = \omega_2(r)$ from the above assumptions. Then, again from (4.3) for ω_2, we conclude

$$\omega_2 = K_1' \log r + K_2'$$

for additional constants K_1', K_2'. But again, from the single-valuedness of pressure, we have $K_1' = 0$ and $\omega_2 = K_2'$. This argument is generalized to characterize ω_n, $n \geq 1$, and establish the principle by induction. Thus, we suppose each ω_n is constant.

4.2. 1st order outer expansion: Euler flow. We calculate the asymptotic expansion of the flow when the outer wall velocity is slightly perturbed from rigid rotation. This approach simplifies our analysis of the effects of finite $R \gg 1$ and allows us to compare the asymptotic results with numerical computations later on. In our numerical computations, we also consider other scenarios, including perturbations to the inner wall velocity and perturbations to both wall velocities.

Let us fix $r_2 = 1$ and vary r_1 for the convenience. We suppose initially a solid body rotation of the flow with the outer wall speed 1 in the given annulus. This is also a simple example of Taylor-Couette flow in an annular domain. Then we perturb the flow with the outer wall velocity

$$u_r(1,\theta) = 0, \quad u_\theta(1,\theta) = 1 + \epsilon f(\theta)$$

for a small $\epsilon > 0$. Here $f(\theta) = \sum_{n\neq 0} c_n e^{in\theta}$, $c_n = \overline{c_{-n}}$ and has zero average along the wall. All the complex summations below are done with the positive and the negative indices in pair. Taking the curvilinear coordinate x, y along the circular wall i.e. x for θ and y for $r_2 - r = 1 - r$, we use $\Psi_k, U, V, P, Y, \Delta_k$ for outer variables and $\psi_k, u, v, p, y, \delta_k$ for inner variables.

The equations for the outer expansion in curvilinear coordinate (x, y) are

$$(\mathbf{u}\cdot\nabla - R^{-1}\nabla^2)\nabla^2\Psi = 0 \tag{4.5}$$

$$\Psi(x,0) = 0, \quad \Psi_y(x, 1-r_1) = r_1 = q_{e1} \tag{4.6}$$

where $\mathbf{u} = (-\partial\Psi/\partial r, \partial\Psi/(r\partial\theta))$. We start with the outer expansion as $R \to \infty$,

$$\begin{aligned}(\Psi, u, v, p, \omega)(x, y; R) \sim{}& \Delta_1(R)(\Psi_1, U_1, V_1, P_1, \Omega_1)(x, y) \\ &+ \Delta_2(R)(\Psi_2, U_2, V_2, P_2, \Omega_2)(x, y) + \cdots\end{aligned} \tag{4.7}$$

For the 1st order terms, we take $\Delta_1(R) = 1$ and $\Omega_1(\Psi_1) = \Omega_1(r)$ from PB theory. Here BW formula yields

$$\Omega_1 = 2 + \frac{1}{1 - r_1^2}\sum_{n\neq 0} |c_n|^2\epsilon^2 + O(\epsilon^3), \tag{4.8}$$

from which we obtain the 1st order terms of the expansions,

$$\Psi_1(x, y; \epsilon) = -\left[\frac{1}{2} + \frac{1}{4(1-r_1^2)}\sum_{n\neq 0}|c_n|^2\epsilon^2\right] r^2 - \frac{r_1^2}{2(1-r_1^2)}\sum_{n\neq 0}|c_n|^2\epsilon^2 \log r + O(\epsilon^3),$$

$$U_1(x, y; \epsilon) = \left[1 + \frac{1}{2}\sum_{n\neq 0}|c_n|^2\epsilon^2\right] r + \frac{r_1^2}{2(1-r_1^2)}\sum_{n\neq 0}|c_n|^2\epsilon^2\frac{1}{r} + O(\epsilon^3),$$

$$V_1(x, y; \epsilon) = 0.$$

4.3. First order inner expansion: The boundary layer equation. The Navier–Stokes equations under the curvilinear coordinates (x, y) are given in [29] by

$$\frac{\partial u}{\partial x} + (1+\kappa y)\frac{\partial v}{\partial y} + \kappa v = 0, \tag{4.9}$$

$$\begin{aligned}\frac{u}{h_1}\frac{\partial u}{\partial x} + v\frac{\partial u}{\partial y} + \frac{\kappa uv}{h_1} &= -\frac{1}{\rho h_1}\frac{\partial p}{\partial x} \\ &+ \frac{1}{R}\left(\frac{1}{{h_1}^2}\frac{\partial^2 u}{\partial x^2} + \frac{\partial^2 u}{\partial y^2} + \frac{2\kappa}{{h_1}^2}\frac{\partial v}{\partial x} + \frac{\kappa' y}{{h_1}^2}\frac{\partial v}{\partial y} + \frac{\kappa}{h_1}\frac{\partial u}{\partial y} - \frac{\kappa^2}{{h_1}^2}u + \frac{\kappa'}{{h_1}^2}v\right),\end{aligned} \tag{4.10}$$

$$\begin{aligned}\frac{u}{h_1}\frac{\partial v}{\partial x} + v\frac{\partial v}{\partial y} - \frac{\kappa u^2}{h_1} &= -\frac{1}{\rho}\frac{\partial p}{\partial y} \\ &+ \frac{1}{R}\left(\frac{1}{{h_1}^2}\frac{\partial^2 v}{\partial x^2} + \frac{\partial^2 v}{\partial y^2} + \frac{2\kappa}{h_1}\frac{\partial v}{\partial y} - \frac{\kappa}{{h_1}^2}\frac{\partial u}{\partial x} - \frac{\kappa' y}{{h_1}^3}\frac{\partial v}{\partial x} - -\frac{\kappa' u}{{h_1}^3}\right).\end{aligned} \tag{4.11}$$

Here $h_1 = 1+\kappa y$ and $\kappa = -1$, $\kappa' = d\kappa/dx = 0$, $\rho = 1$ in the present case. Below we always simplify the calculation using these specific values.

For the inner expansion, we suppose

$$\begin{aligned}(\psi, u, v, p, \omega)(x, y; R) \sim{}& \delta_1(R)(\psi_1, u_1/\delta_1(R), v_1, p_1/\delta_1(R), \omega_1/{\delta_1}^2(R))(x, Y) \\ &+ \delta_2(R)(\psi_2, u_2/\delta_1(R), v_2, p_2/\delta_1(R), \omega_2/{\delta_1}^2(R))(x, Y) + \cdots\end{aligned}$$

as $R \to \infty$, x, Y fixed, where $Y = y/\delta_1(R)$ is an extended coordinate in the boundary layer. Immediately we obtain $\delta_1(R) = 1/\sqrt{R}$ and $\delta_2(R) = 1/R$ from the principle of nondegeneracy. Inserting these expansions into the above and collecting the $O(1)$ terms, we obtain the same boundary layer equation for the flat wall case. Proper boundary conditions are found by matching $u_1(x, \infty; \epsilon)$ with $U_1(x, 0; \epsilon)$, and the problem becomes

$$\frac{\partial u_1}{\partial x} + \frac{\partial v_1}{\partial Y} = 0, \quad u_1\frac{\partial u_1}{\partial x} + v_1\frac{\partial u_1}{\partial Y} - \frac{\partial^2 u_1}{\partial Y^2} = 0, \tag{4.12}$$

$$u_1(x, 0; \epsilon) = 1 + \epsilon\sum_{n\neq 0} c_n e^{inx}, \quad v_1(x, 0; \epsilon) = 0, \tag{4.13}$$

$$u_1(x, \infty; \epsilon) = 1 + \frac{1}{2}\sum_{n\neq 0} |c_n|^2\epsilon^2 + \cdots. \tag{4.14}$$

We assume the expansion of the solution $u_1(x, Y; \epsilon), v_1(x, Y; \epsilon)$ in ϵ as the following:

$$(u_1, v_1)(x, Y; \epsilon) = (u_{10}, v_{10})(x, Y) + \epsilon(u_{11}, v_{11})(x, Y) + \epsilon^2(u_{12}, v_{12})(x, Y) + \cdots.$$

These are substituted into (4.12)–(4.14) and the $O(1)$ terms give,

$$u_{10}(x, Y) = 1,\ v_{10}(x, Y) = 0,\ \omega_{10}(x, Y) = 0. \tag{4.15}$$

For $O(\epsilon)$ terms, a similar procedure yields

$$\frac{\partial u_{11}}{\partial x} + \frac{\partial v_{11}}{\partial Y} = 0, \quad u_{10}\frac{\partial u_{11}}{\partial x} - \frac{\partial^2 u_{11}}{\partial Y^2} = 0, \tag{4.16}$$

$$u_{11}(x, 0) = \sum_{n\neq 0} c_n e^{inx}, \quad v_{11}(x, 0) = u_{11}(x, \infty) = 0, \tag{4.17}$$

and

$$u_{11}(x,Y)=\sum_{n\neq 0} c_n e^{inx-\sqrt{in}Y}, \quad v_{11}(x,Y)=\sum_{n\neq 0} c_n\sqrt{in}e^{inx}[e^{-\sqrt{in}Y}-1]. \tag{4.18}$$

Third, working with the $O(\epsilon^2)$ terms, we have

$$\frac{\partial u_{12}}{\partial x}+\frac{\partial v_{12}}{\partial Y}=0, \quad u_{10}\frac{\partial u_{12}}{\partial x}+u_{11}\frac{\partial u_{11}}{\partial x}+v_{11}\frac{\partial u_{11}}{\partial Y}-\frac{\partial^2 u_{12}}{\partial Y^2}=0, \tag{4.19}$$

$$u_{12}(x,0)=v_{12}(x,0)=0, \quad u_{12}(x,\infty)=\frac{1}{2}\sum_{n\neq 0}|c_n|^2. \tag{4.20}$$

Then, we solve to obtain,

$$\begin{aligned} u_{12}(x,Y)=&-\sum_{n,m\neq 0} c_n c_m \left\{ \frac{(\sqrt{in}\sqrt{im}-im)}{2\sqrt{in}\sqrt{im}}\left(e^{-(\sqrt{in}+\sqrt{im})Y}-e^{-\sqrt{i(n+m)}Y}\right)\right.\\ &\left.+\frac{\sqrt{im}}{\sqrt{in}}\left(e^{-\sqrt{im}Y}-e^{-\sqrt{i(n+m)}Y}\right)\right\}e^{i(n+m)x},\\ v_{12}(x,Y)=&\sum_{n,m\neq 0} c_n c_m \left[\frac{(\sqrt{in}\sqrt{im}-im)}{2\sqrt{in}\sqrt{im}}\left\{-\frac{i(m+n)}{\sqrt{in}+\sqrt{im}}(e^{-(\sqrt{in}+\sqrt{im})Y}-1)\right.\right.\\ &\left.+\sqrt{i(n+m)}(e^{-\sqrt{i(n+m)}Y}-1)\right\}-\frac{i(m+n)}{\sqrt{in}}[e^{-\sqrt{im}Y}-1]\\ &\left.+\sqrt{i(n+m)}\frac{\sqrt{im}}{\sqrt{in}}(e^{-\sqrt{i(n+m)}Y}-1)\right]e^{i(n+m)x}. \end{aligned}$$

4.4. Second order outer expansion. For the next order terms, we need to incorporate the displacement thickness phenomenon. Namely, the normal velocity of the first order inner expansion does not vanish outside the boundary layer and thus modifies the outer flow.

From the matching order condition,

$$\delta_1(R)\psi_{1x}(x,\infty)=\Delta_2(R)\Psi_{2x}(x,0), \tag{4.21}$$

we derive $\Delta_2(R)=1/\sqrt{R}$. For $\Psi_2(x,y)$, substituting the outer expansion (4.7) into the full equation (4.5) yields a linear equation for Ψ_2,

$$(U_1,V_1)\cdot\nabla(\nabla^2\Psi_2)+(U_2,V_2)\cdot\nabla(\nabla^2\Psi_1)=\nabla^2\nabla^2\Psi_1. \tag{4.22}$$

Here the second term, representing the convection of the first order vorticity along the second order corrections to the streamlines, does not vanish in general. This makes it more difficult to proceed than the flat plate or disk flow case [18].

However, assuming Ψ_2 as a function of r only when unperturbed, the second term vanishes identically and we find that Ω_2 is a linear function of $\log r$. This result is consistent with the principle of transcendental decay in section 4.1. Consequently, the problem for $\Psi_2(x,y)$ becomes

(4.23)

$$\nabla^2\Psi_2 = K_2', \quad \Psi_2(x,0)=0,$$
$$\Psi_{2x}(x,0) = \left(\sum_{n\neq 0} c_n\sqrt{in}e^{inx}\right)\epsilon - \left[\sum_{n,m\neq 0} c_nc_me^{i(n+m)x}\left\{\frac{(\sqrt{in}\sqrt{im}-im)}{2\sqrt{in}\sqrt{im}}\right.\right.$$
$$\left.\left.\times\left(\frac{i(m+n)}{\sqrt{in}+\sqrt{im}}-\sqrt{i(n+m)}\right)+\frac{i(m+n)}{\sqrt{in}} - \sqrt{i(n+m)}\frac{\sqrt{im}}{\sqrt{in}}\right\}\right]\epsilon^2.$$

Here Ω_2 is the second order vorticity which has the expansion

$$\Omega_2(x,y;\epsilon) = \Omega_{20}(x,Y)+\Omega_{21}(x,Y)\epsilon+\Omega_{22}(x,Y)\epsilon^2+\cdots. \tag{4.24}$$

From the result of section 4.1, we put all $\Omega_{20}(x,Y),\Omega_{21}(x,Y),\dots$ as some fixed constants. We may set $\Omega_{20}=0$ immediately, since Ω_{20} represents a viscous correction, and for $\epsilon=0$, there is no boundary layer. This will be verified explicitly in the solution of the second order inner expansion problem. For $\Omega_{21},\Omega_{22},\dots$, the second order inner expansion should determine these functions from the principle of transcendental decay and the BW formula. This differs from the Blasius problem, where the external vorticity is known in advance to be zero to all orders; see [30].

Solving (4.23), we obtain

$$\Psi_2(x,y) = \left(B_{21}(1-y)^2+C_{21}\log(1-y)+\sum_{n\neq 0}\frac{c_n}{\sqrt{in}}e^{inx}[(1-y)^{|n|}-r_1^{|n|}]\right)\epsilon$$
$$-\left[B_{22}(1-y)^2+C_{22}\log(1-y)\right.$$
$$+\sum_{\substack{n,m\neq 0\\ n+m\neq 0}} c_nc_m\left\{\frac{(\sqrt{in}\sqrt{im}-im)}{2\sqrt{in}\sqrt{im}}\left(\frac{1}{\sqrt{in}+\sqrt{im}}-\frac{1}{\sqrt{i(n+m)}}\right)\right.$$
$$\left.\left.+\frac{1}{\sqrt{in}}-\frac{\sqrt{im}}{\sqrt{in}\sqrt{i(n+m)}}\right\}\times[(1-y)^{|m+n|}-r_1^{|m+n|}]e^{i(n+m)x}\right]\epsilon^2$$

for some constants $B_{21},B_{22},C_{21},C_{22}$. Thus

$$U_2(x,y;\epsilon) = \left(-2B_{21}(1-y)-\frac{C_{21}}{1-y}-\sum_{n\neq 0}\frac{c_n|n|}{\sqrt{in}}e^{inx}(1-y)^{|n|-1}\right)\epsilon$$
$$+\left[-2B_{22}(1-y)-\frac{C_{22}}{1-y}\right.$$
$$+\sum_{\substack{n,m\neq 0\\ n+m\neq 0}} c_nc_m\left\{\frac{(\sqrt{in}\sqrt{im}-im)}{2\sqrt{in}\sqrt{im}}\left(\frac{1}{\sqrt{in}+\sqrt{im}}-\frac{1}{\sqrt{i(n+m)}}\right)\right.$$
$$\left.\left.+\frac{1}{\sqrt{in}}\left(1-\frac{\sqrt{im}}{\sqrt{i(n+m)}}\right)\right\}|m+n|(1-y)^{|m+n|-1}e^{i(n+m)x}\right]\epsilon^2.$$

4.5. Second order inner expansion. Next we proceed to the second order boundary layer equation. Gathering the $O(1/\sqrt{R})$ terms in the curvilinear Navier–Stokes equations (4.9)–(4.11), we have the following equations for u_2, v_2, p_2:

$$\frac{\partial u_2}{\partial x}+\frac{\partial v_2}{\partial Y}=\frac{\partial}{\partial Y}(v_1 Y),\quad \frac{\partial p_2}{\partial Y}=-{u_1}^2, \tag{4.25}$$

$$\begin{aligned} u_1\frac{\partial u_2}{\partial x}+v_1\frac{\partial u_2}{\partial Y}+u_2\frac{\partial u_1}{\partial x}+v_2\frac{\partial u_1}{\partial Y}&=-\frac{\partial p_2}{\partial x}+\frac{\partial^2 u_2}{\partial Y^2}\\ &\quad-\left\{Y\left(u_1\frac{\partial u_1}{\partial x}+\frac{\partial p_1}{\partial x}\right)+\frac{\partial u_1}{\partial Y}-u_1v_1\right\}. \end{aligned} \tag{4.26}$$

We apply the matching principle for the first two terms in the expansions of $u(x,y)$ to obtain

$$[-YU_1(x,0)+U_2(x,0)]\,\frac{1}{\sqrt{R}}=u_2(x,\infty)\delta_2(R)\sqrt{R}. \tag{4.27}$$

Thus $\delta_2(R)=1/R$ and as $Y\to\infty$,

$$\begin{aligned} u_2(x,Y;\epsilon)&=-Y\,U_1(x,0;\epsilon)+U_2(x,0;\epsilon)\\ &=-Y-\left(2B_{21}+C_{21}+\sum_{n\neq 0}c_n\frac{|n|}{\sqrt{in}}e^{inx}\right)\epsilon\\ &\quad+\left[-\frac{1}{2}Y\sum_{n\neq 0}|c_n|^2-2B_{22}+C_{22}\right.\\ &\quad+\sum_{\substack{n,m\neq 0\\ n+m\neq 0}}c_nc_m\left\{\frac{(\sqrt{in}\sqrt{im}-im)}{2\sqrt{in}\sqrt{im}}\left(\frac{1}{\sqrt{in}+\sqrt{im}}-\frac{1}{\sqrt{i(n+m)}}\right)\right.\\ &\quad\left.\left.+\frac{1}{\sqrt{in}}-\frac{\sqrt{im}}{\sqrt{in}\sqrt{i(n+m)}}\right\}|m+n|e^{i(n+m)x}\right]\epsilon^2. \end{aligned}$$

By a similar matching procedure on the pressure $p(x,y)$, we have the condition for $p_2(x,Y)$ as $Y\to\infty$:

$$\begin{aligned} p_2(x,Y)&\sim Y\frac{\partial P_1}{\partial y}(x,0)+P_2(x,0)\\ &=-Y+\left(C_{21}+\sum_{n\neq 0}\frac{c_n}{\sqrt{in}}(|n|-2)e^{inx}\right)\epsilon+O(\epsilon^2). \end{aligned}$$

(See Appendix A.1 for the computation of P_1, P_2.) Let us assume that the second term of the inner expansions is expanded by

$$(u_2,v_2,p_2,\omega_2)(x,Y;\epsilon)=(u_{20},v_{20},p_{20},\omega_{20})(x,Y)+\epsilon(u_{21},v_{21},p_{21},\omega_{21})(x,Y)+\cdots.$$

At this stage, averaging over x for $(0,2\pi)$ simplifies the calculation and we obtain the result on the following second order vorticity:

$$\Omega_{20}=0,\quad \Omega_{21}=0,\quad 2B_{22}+C_{22}=-2\sum_{n>0}|c_n|^2\frac{4-n}{\sqrt{2n}}. \tag{4.28}$$

(Details of the calculation are in Appendix A.2.) In particular, if $f(x) = \sin x$, we compute

$$2B_{22} + C_{22} = -\frac{3\sqrt{2}}{4}. \tag{4.29}$$

Therefore, from the boundary condition at r_1, we fully determine

$$\Omega_{22} = 2\sqrt{2}. \tag{4.30}$$

5. Numerical method. From the geometry, we introduce the polar coordinate $(r, \theta) \in [r_1, r_2] \times [0, 2\pi]$ to rewrite the steady state stream-function–vorticity formulation as

$$\frac{\partial^2 \psi}{\partial r^2} + \frac{1}{r}\frac{\partial \psi}{\partial r} + \frac{1}{r^2}\frac{\partial^2 \psi}{\partial \theta^2} = -\omega, \tag{5.1}$$

$$\frac{\partial^2 \omega}{\partial r^2} + \frac{1}{r}\frac{\partial \omega}{\partial r} + \frac{1}{r^2}\frac{\partial^2 \omega}{\partial \theta^2} = \frac{R}{r}\left(\frac{\partial \psi}{\partial \theta}\frac{\partial \omega}{\partial r} - \frac{\partial \psi}{\partial r}\frac{\partial \omega}{\partial \theta}\right) \tag{5.2}$$

with the physical boundary conditions

$$u_r(r_i, \theta) = \frac{1}{r}\frac{\partial \psi}{\partial \theta}(r_i, \theta) = 0, \quad u_\theta(r_i, \theta) = -\frac{\partial \psi}{\partial r}(r_i, \theta) = g(r_i, \theta) \tag{5.3}$$

for some given function g along the boundaries $r = r_1, r = r_2$. Note that the two disconnected boundaries are natural streamlines and we may set $\psi(r_2) = 0$. It is worth noting that the value of ψ on the inner boundary $r = r_1$ is unknown at this stage although it should be a constant. Accordingly, using the boundary velocity conditions, we may set up the corresponding boundary conditions for ψ as follows,

$$\psi(r_1, \theta) = c, \quad -\frac{\partial \psi}{\partial r}(r_1, \theta) = g(r_1, \theta), \tag{5.4}$$

$$\psi(r_2, \theta) = 0, \quad -\frac{\partial \psi}{\partial r}(r_2, \theta) = g(r_2, \theta), \tag{5.5}$$

where c is an unknown constant. Here, we use the single-valued condition (3.11) for ψ on $r = r_1$ in subsection 3.1 in order to solve the coupled system (5.1) and (5.2) (and determine c).

Specifically, we utilize a fast high order numerical method using an adaptive scheme [20]. Namely, we further expand ψ, ω in Fourier-mode form with $\psi_{-k}(r) = \overline{\psi_k(r)}$ and $\omega_{-k}(r) = \overline{\omega_k(r)}$,

$$\psi(r, \theta) = \sum_{k=-N}^{N} \psi_k(r) e^{ik\theta}, \quad \omega(r, \theta) = \sum_{k=-N}^{N} \omega_k(r) e^{ik\theta}, \tag{5.6}$$

and obtain the relation for each mode $k = 0, \ldots, N$,

$$\psi_k'' + \frac{1}{r}\psi_k' - \frac{k^2}{r^2}\psi_k = -\omega_k, \tag{5.7}$$

$$\omega_k'' + \frac{1}{r}\omega_k' - \frac{k^2}{r^2}\omega_k = \frac{R}{r}\sum_{l+m=k} il(\psi_l \omega_m' - \psi_m' \omega_l). \tag{5.8}$$

Here the boundary conditions for $\psi(r)$ can be easily obtained from (5.4) and (5.5):

$$-\psi_0'(r_1) = g_0(r_1), \quad \psi_0(r_2) = 0, \tag{5.9}$$

$$\psi_k(r_1) = 0, \qquad \psi_k(r_2) = 0, \quad k = 1, \ldots, N. \tag{5.10}$$

Additionally from the tangential components of the boundary velocity $g(r_i, \theta)$, we have overimposed the boundary condition on $\psi_k'(r)$,

$$g(r_i, \theta) = \sum_{k=-N}^{N} g_k(r_i)\, e^{ik\theta} = -\sum_{k=-N}^{N} \psi_k'(r_i)\, e^{ik\theta}. \tag{5.11}$$

Next, we implement an explicit iterative scheme on these coupled Poisson equations (5.7) and (5.8). First, ψ_k in (5.7) are updated from the previous ω_k for all k with boundary conditions (5.9) and (5.10). And then ω_k in (5.8) are updated using the updated $\psi_{i=0,\ldots,N}$, $\omega_{i=0,\ldots,k-1}$, and the previous $\omega_{i=k,\ldots,N}$. Here boundary values of ω_k are given using a McLaurin-type condition [23]:

$$\omega = -\nabla^2 \psi + \beta \left[\frac{\partial \psi}{\partial n} + g \right] \text{ on } \{(r_i, \theta) : i = 1, 2\} \tag{5.12}$$

for some proper constant β. We set $\beta = \beta_0 / r_i$ for current computations. Now the resulting equation becomes a Bessel-like second order differential equation (5.8) with two proper boundary conditions at $r = r_1$ and $r = r_2$,

$$\omega_0'(r_1) = 0, \quad \omega_0(r_2) = -\psi_0''(r_2) - \frac{1}{r_2}\psi_0'(r_2) + \frac{\beta_0}{r_2}\left(\psi_0'(r_2) + g_0(r_2)\right), \tag{5.13}$$

$$\omega_k(r_i) = -\psi_k''(r_i) - \frac{1}{r_i}\psi_k'(r_i) \mp \frac{\beta_0}{r_i}\left(\psi_k'(r_i) + g_k(r_i)\right) \tag{5.14}$$

for $k > 0$. Here, we use the single-valuedness condition, $\omega_0'(r_1) = 0$ instead of imposing the given boundary velocity condition with $g_0(r_1)$ which is already used in (5.9).

We remark that once an iterative solution of the system of ordinary differential equations (5.7) and (5.8) using the boundary conditions (5.9), (5.10), (5.13), and (5.14) reaches a consistent stage, the order of spatial accuracy of the solution solely depends on the order of accuracy of $\nabla^2\psi$ and $\partial\psi/\partial n$. Therefore, the computational result guarantees the same order of accuracy with the integral equation solver and an eighth order method are used for the simulations in the following section.

The Stokes iteration [20], which solves (5.7) and (5.8) alternatively as described above, with the convection terms explicitly computed from previous iterations converges fairly well for $R \leq 100$. However, the number of iterations increases as the Reynolds number becomes large, and the numerical solution may blow up without additional care. To compute the flow for significantly larger Reynolds numbers, such as $R = 10000$, we employ a continuation procedure [20]. We start by computing the solution at a relatively small Reynolds number and gradually increase the Reynolds number after reaching a steady state, allowing us to achieve another steady state, and so on. For large perturbations, we find that a more refined continuation method is necessary.

6. Numerical results and discussion. For the confirmation and validity of the theory developed above, we numerically compute a few practical perturbed cases. Let us set $r_1 = 1/2, r_2 = 1$. For all cases, we begin with the basic flow of solid body rotation,

$$\psi = -(r^2-1)/2,\ u_\theta = r,\ \omega = 2, \tag{6.1}$$

where we put $A = 0$, $B = -1/2$ in (3.3). In the computation below, we first take

$$q_1 = 1/2, \quad q_2 = 1 + \epsilon \sin\theta, \tag{6.2}$$

where ϵ represents the magnitude of perturbation and is taken small enough for the stability of the flow and with no reverse flow. This is a perturbation of the solid body rotation with only the outer boundary velocity. Later, we also try the perturbed case by both the inner and outer boundary velocity. For this, we put

$$q_1 = 1/2 + \epsilon_1 \sin\theta + \epsilon_2 \cos\theta, \quad q_2 = 1 + \epsilon \sin\theta, \tag{6.3}$$

where ϵ represents the magnitude of the outer perturbation, while ϵ_1 and ϵ_2 represent the in-phase and quadrature-phase components of the inner perturbation.

6.1. Boundary layers for high Reynolds number flows. During the computation, we encounter a significant difficulty related to the potential emergence of boundary layers near the two walls. As we increase the Reynolds number, a thin boundary layer forms that must be resolved accurately in our numerical calculations. To address this, an adaptive method [20] has already been developed, demonstrating both effectiveness and accuracy.

In this paper, we modify and adapt this method for multiply connected domains. This adaptation requires solving the Poisson equation for an annulus, which presents a difficulty in imposing boundary conditions on both walls. This issue has been previously discussed in [22], and appropriate techniques have been developed to overcome these difficulties. We summarize our results through the following eight experiments.

Experiment 1 (spectral convergence for large Reynolds numbers).

In this experiment, we check how many Fourier modes are needed to resolve the high Reynolds number flows for $R = 100, 1000, 10000$. Figure 1 displays the relative L_2-norm of ω_k, $\frac{\|\omega_k(\cdot)\|}{\|\omega_0(\cdot)\|}$, $k = 1, \ldots, N$, for (6.2) with $\epsilon = 0.02, 0.2$. We note that the amplitudes of the higher modes are exponentially decaying so the method is spectrally accurate in angular direction. The number of frequency modes to resolve

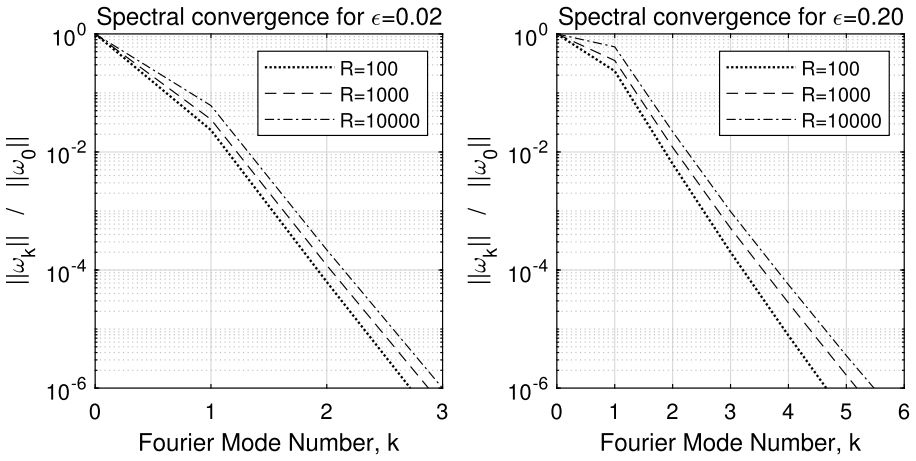

FIG. 1. *Spectral convergence of Fourier modes: Relative L_2-norm of ω_k for $q_1 = 1/2, q_2 = 1 + \epsilon \sin\theta$ with $\epsilon = 0.02, 0.2$.*

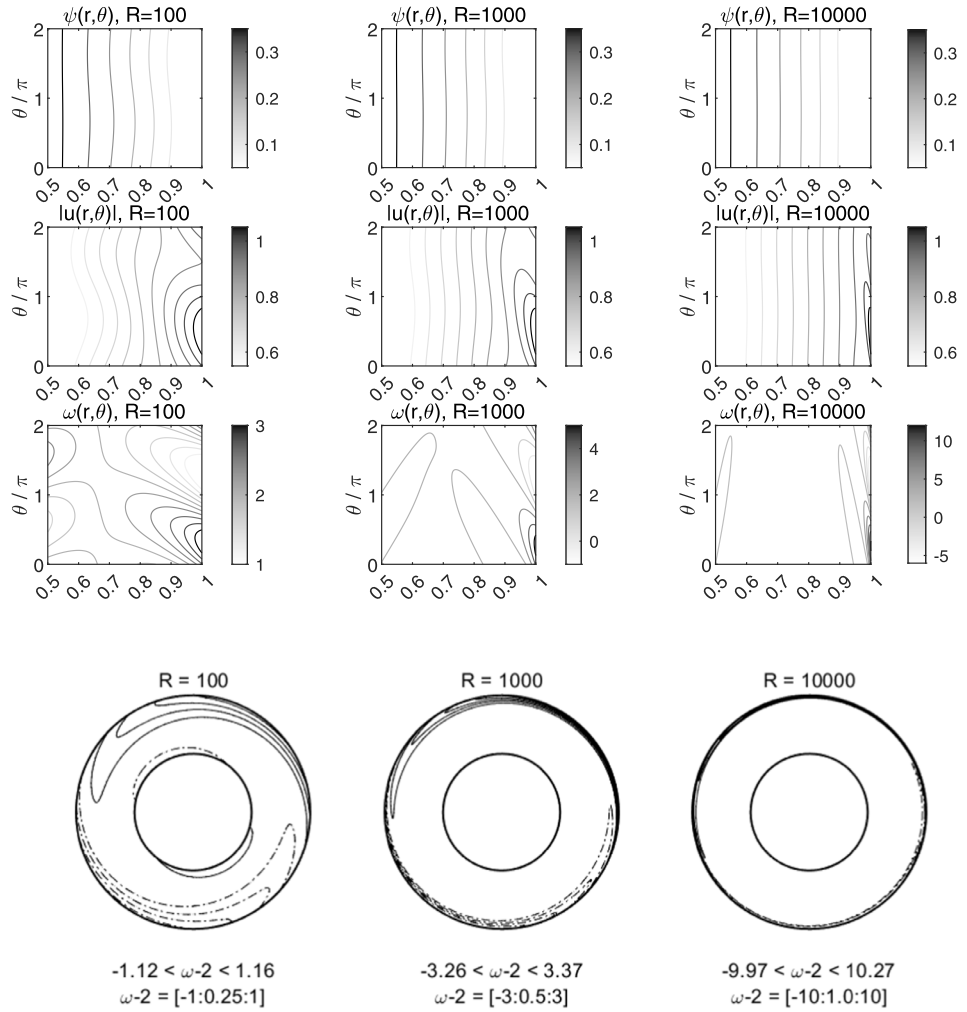

FIG. 2. *Streamline, velocity, and vorticity distribution in contour lines for* $q_1 = 1/2$, $q_2 = 1 + 0.1\sin\theta$. *Solid and solid-dotted contour lines on the annulus domain represent* $\omega > 2$ *and* $\omega < 2$, *respectively, while the spacing and the range of* ω *are given on the bottom.*

the computation increases for the higher Reynolds number and larger perturbation cases. However, we found that 16 modes are enough to guarantee single precision accuracy for most of performed simulations with $\epsilon \leq 0.1$, $R \leq 10000$.

Experiment 2 (streamline and vorticity for the outer perturbation).

We begin to discuss the numerical result for the outer perturbation case with $\epsilon = 0.1$ and $\epsilon_1 = \epsilon_2 = 0$. In Figure 2, the stream function $\psi(r, \theta)$ shown on the top row smoothly increases from 0 to 3/8 as moving inward. The speed $||\mathbf{u}(r, \theta)||$ on the inner wall is about 1/2 while it varies from 0.9 to 1.1 on the outer wall, as expected.

The vorticity distribution $\omega(r, \theta)$ presented in the bottom row is particularly intriguing. Figure 2 also displays the contour lines of the vorticity distribution for various R values in the annular domain. Here, we clearly observe a thin layer emerging near the outer boundary $r_2 = 1$ as R increases, along with a rapid increase in both the strength and fluctuations of the vorticity in that region.

It is noteworthy that the vorticity on the inner boundary $r_1 = 1/2$ (without speed perturbation on the boundary) varies significantly, while the vorticity in the bulk region of the domain approaches $\omega = 2$ as R increases. The plots in the left column for $R = 100$ clearly demonstrate fluctuations in vorticity, even in the absence of boundary velocity perturbations. However, for larger R, it becomes less evident to observe this phenomenon on the inner wall, as the relative magnitude of the fluctuations increases substantially on the outer boundary

In Experiment 3, we will quantitatively analyze the strength of the vorticity fluctuations and the thickness of the layer as functions of R.

Experiment 3 (vorticity profile for various Reynolds numbers).

In order to determine the thickness and the strength of the vorticity layers, we consider three different perturbation cases:

(i) outer layer only (top): $q_1 = 1/2$, $q_2 = 1 + 0.1 \sin\theta$;

(ii) both layers (middle): $q_1 = 1/2 + 0.1\cos\theta$, $q_2 = 1 + 0.1\sin\theta$;

(iii) inner layer only (bottom): $q_1 = 1/2 + 0.1\cos\theta$, $q_2 = 1$,

where the corresponding $(\epsilon, \epsilon_1, \epsilon_2) = (0.1, 0, 0), (0.1, 0, 0.1), (0, 0, 0.1)$, respectively.

The upper half plots in Figure 3 show the minimum and the maximum envelop of the vorticity $\omega(r, \cdot)$ as a function of r. We clearly see that the layer becomes thinner and the deviation from limiting constant value $\omega = 2$ becomes larger as R increases. To investigate this phenomenon quantitatively, let us define the strength of the layer to be

$$\max_{0 \le \theta < 2\pi} |\omega(r_i, \theta) - 2| \tag{6.4}$$

for r_1 or r_2 and the thickness of the layer to be the length where the strength becomes half of the averaged boundary vorticity. The second column of the bottom half plots show that the layer strength is $O(\sqrt{R})$ only on the perturbed boundary (top: r_2; middle: r_1, r_2; bottom: r_1) and it is $O(1)$ on the unperturbed boundary whereas the thickness shown on the third column is always $O(1/\sqrt{R})$.

It clearly shows the appearance of the *classical* boundary layer where a discontinuity of velocity appears as $R \to \infty$. In contrast to this, there occurs a boundary layer of $O(1)$-strength and $O(1/\sqrt{R})$-thickness even on the unperturbed boundary (top: r_1; bottom: r_2). This is unexpected and quite interesting as no perturbation is imposed there initially. For this case, the velocity there is supposedly continuous by a simple scaling argument, which is confirmed in the second row of Figure 2. Consequently, in spite of the absence of perturbation, we observe an occurrence of a *weak discontinuity* near the unperturbed boundary in the sense that the vorticity is discontinuous while the velocity is continuous there. We do not know the precise mechanism for this phenomenon, but regard it as an intriguing characteristic of an inviscid limit flow.

6.2. Vorticity profile for outer boundary velocity perturbed. Here we first consider the case of outer boundary velocity perturbed,

$$q_1 = 1/2, \quad q_2 = 1 + \epsilon \sin\theta. \tag{6.5}$$

The corresponding Euler limit flow has the following speed on the inner and outer boundaries,

$$q_{e1} = 1/2, \quad q_{e2} = \sqrt{1 + \epsilon^2/2} \tag{6.6}$$

from the BW formula (3.8). Accordingly, we obtain

$$\omega_1 = 2 + 2\epsilon^2/3 = \Omega_1. \tag{6.7}$$

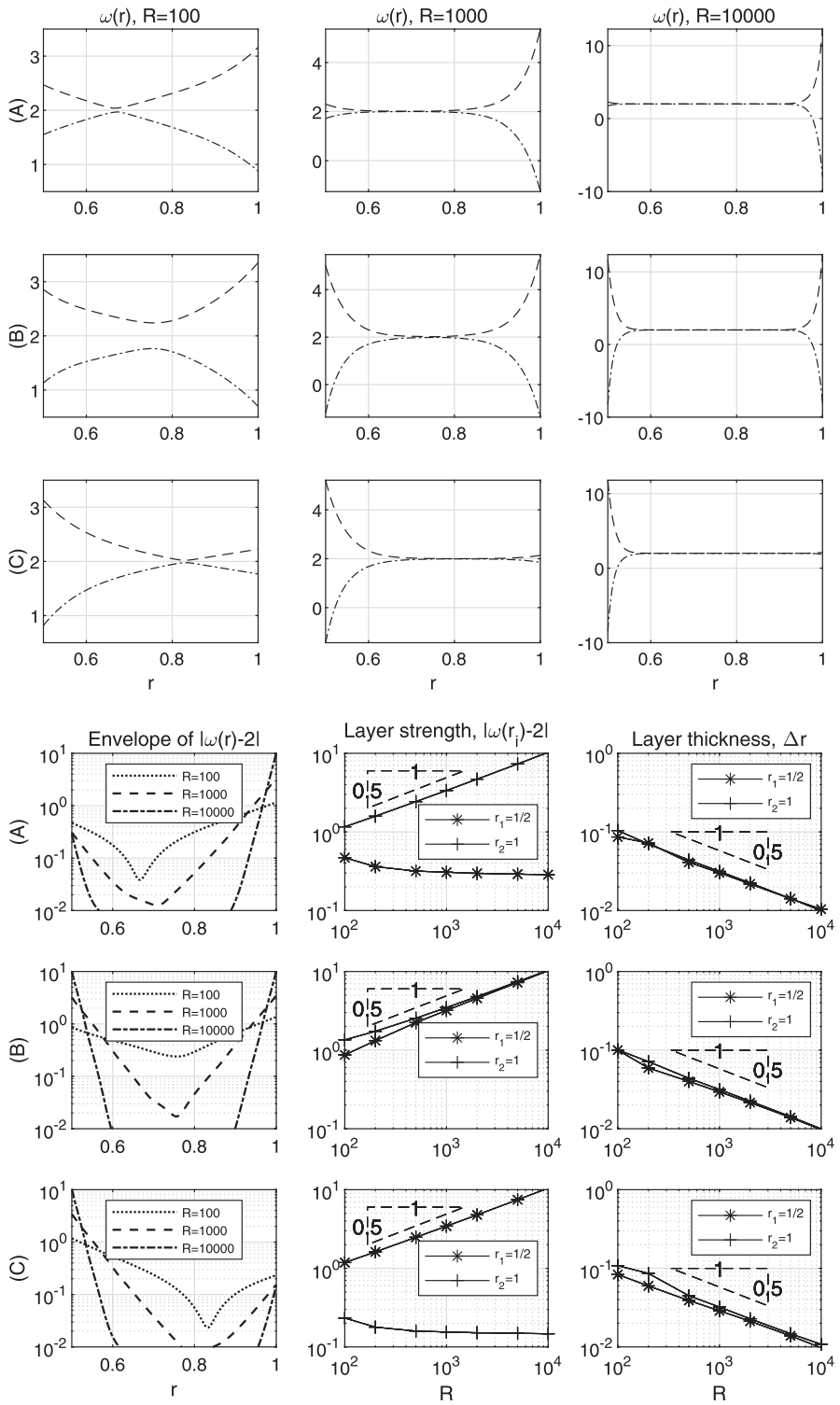

FIG. 3. *Vorticity distribution along r and layer strength/thickness of the layers for outer, both, and inner perturbations cases:* (A) $(\epsilon, \epsilon_1, \epsilon_2) = (0.1, 0, 0)$, (B) $= (0.1, 0, 0.1)$, *and* (C) $= (0, 0, 0.1)$.

This exactly coincides with the first order outer expansion result in (4.8) for $r_1 = 1/2$. Furthermore, considering the finite Reynolds number effect, we obtain the second order outer result as

$$\omega_2 = \Omega_1 + 2\sqrt{2}\frac{\epsilon^2}{\sqrt{R}} \tag{6.8}$$

in section 4. These results are compared with numerical results in the following.

Experiment 4 (velocity u_r, u_θ, and vorticity ω profile with $\epsilon = 0.1$)

Figure 4 shows the velocity $u_r(r,\theta)$, $u_\theta(r,\theta)$, and vorticity $\omega(r,\theta)$ profile for the outer perturbation case (6.5) with $\epsilon = 0.1$. As R increases from 100 to 10000, thin layers emerge on both boundaries. On the inner layer, $u_r(r,\theta)$ becomes smaller while $u_\theta(r,\theta)$ remains at the given velocity 1/2. On the other hand, $\omega(r,\theta)$ approaches a constant (nearly 2) for most of the region as R increases, but the fluctuation along the inner boundary $r_1 = 1/2$ does not decrease as shown at top plots in Figure 4. This supports the emerging of a *weak* boundary layer near the inner wall as commented in Experiment 3.

Along the perturbed outer layer, $u_r(r,\theta)$ becomes smaller and $u_\theta(r,\theta)$ approaches to the given velocity between 0.9 and 1.1. The strength of the vorticity in the layer increases $O(\sqrt{R})$ as described in Experiment 3.

For the following experiments, we take the average of vorticity along a circle $r = c$ to investigate the radial behavior of the vorticity as a function of R and ϵ.

Experiment 5 (radial ω profile for large Reynolds number).

We draw the radial variation of the vorticity mean for $\epsilon = 0.05$ and $\epsilon = 0.1$ in Figure 5, The solid lines are computed values and the dashed or dotted lines are the asymptotic formulas, (6.7) for ω_1 and (6.8) for ω_2. It clearly shows that the average vorticity in the core region becomes constant as R increases and the deviation from constant 2 becomes much larger when ϵ doubles. Another noticeable point is that the average vorticity forms no discontinuity on the inner wall but it becomes discontinuous on the outer wall as R goes to infinity. Here, We also note that ω_2 provides a slightly better approximation of the numerical results compared to ω_1 for larger R.

Experiment 6 (asymptotic formula for $0.02 \le \epsilon \le 0.2$ and $100 \le R \le 1000$).

Figure 6 shows ω as a function of the perturbation strength ϵ and Reynolds number R. Here, we pick a representative of the mean vorticity at $r = 2/3$ to minimize the boundary layer effect for comparison. For various $\epsilon = 0.02, \ldots, 0.2$, the rightmost plot shows scaled vorticity deviation, $|\omega(2/3) - 2| \,/\, \epsilon^2$. We note that the effect of ϵ^2 is clear and the decay patterns for $R > 500$ look similar. For a more detailed comparison and prediction, we draw the right graph in Figure 6. Here we found that the theoretical second order result in (6.7) is a rather good approximation for $R \ge 1000$.

6.3. Vorticity profile for both boundary velocities perturbed. Next, we consider the case when both the inner and the outer velocities are perturbed. Generally, we expect two boundary layers occurring near both boundaries in such cases. Therefore, we can apply the matching method to determine the second order correction of the flow as we did in section 4. This is essentially a local analysis and should be done for both boundaries independently. However, the calculation is very messy and we just use the corresponding first order BW formula instead. For the boundary conditions in (6.3), it immediately follows that

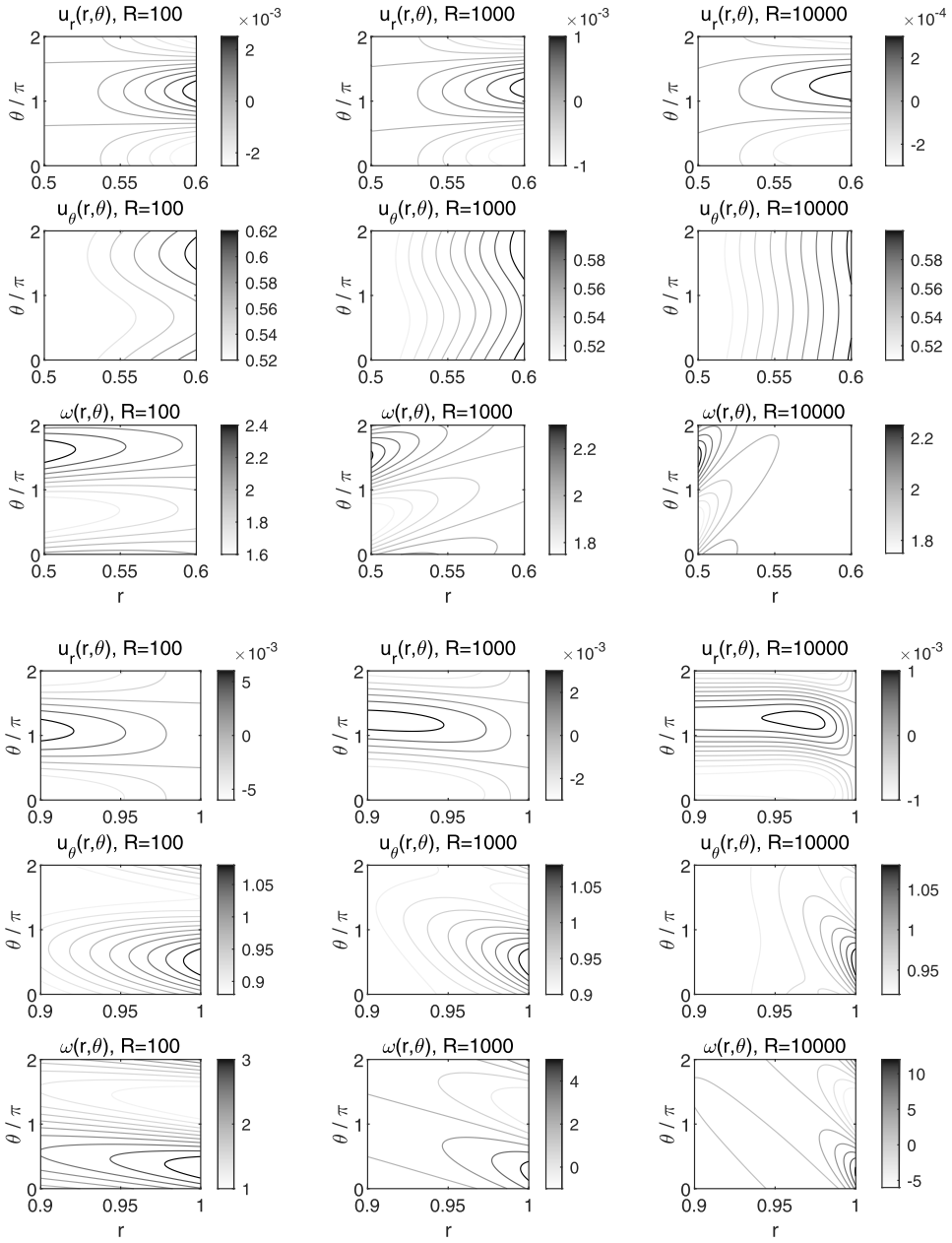

FIG. 4. *Velocity u_r, u_θ and vorticity near the walls $r_1 = 1/2 \le r \le 0.6$ (top) or $0.9 \le r \le r_2 = 1$ (bottom) with $q_1 = 1/2$, $q_2 = 1 + 0.1 \sin\theta$.*

$$q_{e1} = \sqrt{\frac{1}{4} + \frac{\epsilon_1^2 + \epsilon_2^2}{2}}, \quad q_{e2} = \sqrt{1 + \frac{\epsilon^2}{2}}. \tag{6.9}$$

The corresponding BW formula (3.12) yields

$$\omega_1 = 2 + 2(\epsilon^2 - \epsilon_1^2 - \epsilon_2^2)/3. \tag{6.10}$$

These will be compared to numerical results below.

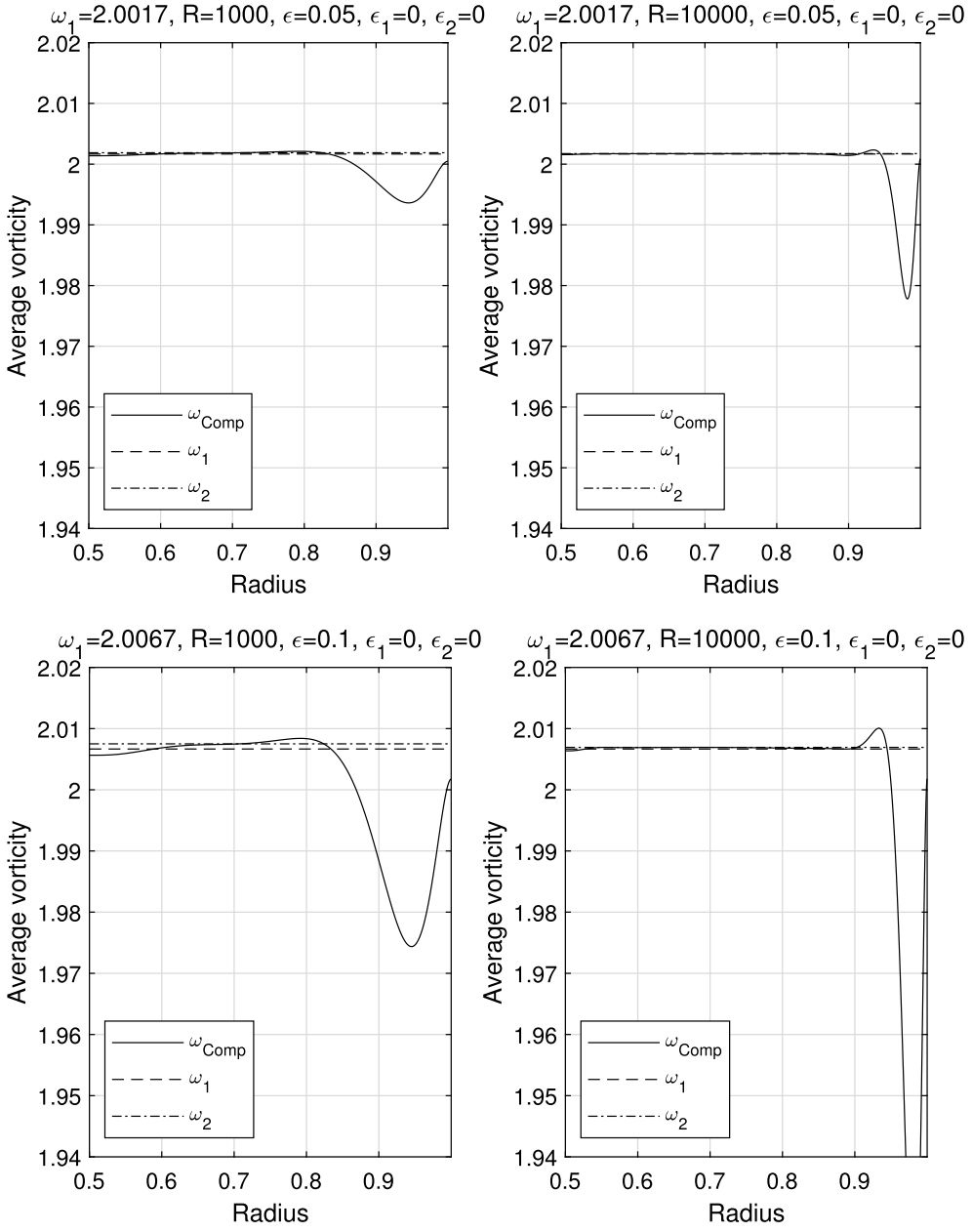

FIG. 5. *Vorticity profiles for steady state along r for* R =1000 *(left),* 10000 *(right), and* $q_1 = 1/2$, $q_2 = 1 + \epsilon \sin\theta$ *with* $\epsilon = 0.05$ *(top),* 0.1 *(bottom).*

Experiment 7 (vorticity profile for both inner and outer perturbations).

Figure 7 shows the radial vorticity variation for $(\epsilon, \epsilon_1, \epsilon_2) = (0.1, 0, 0.05)$, where four curves are computed values for various $R = 1000, 2000, 5000, 10000$ and the constant solid line is the asymptotic formulas (6.10) for ω_1. We note that there form layers in the vorticity near the walls $r_1 = 1/2$ or $r_2 = 1$ and the result seems roughly

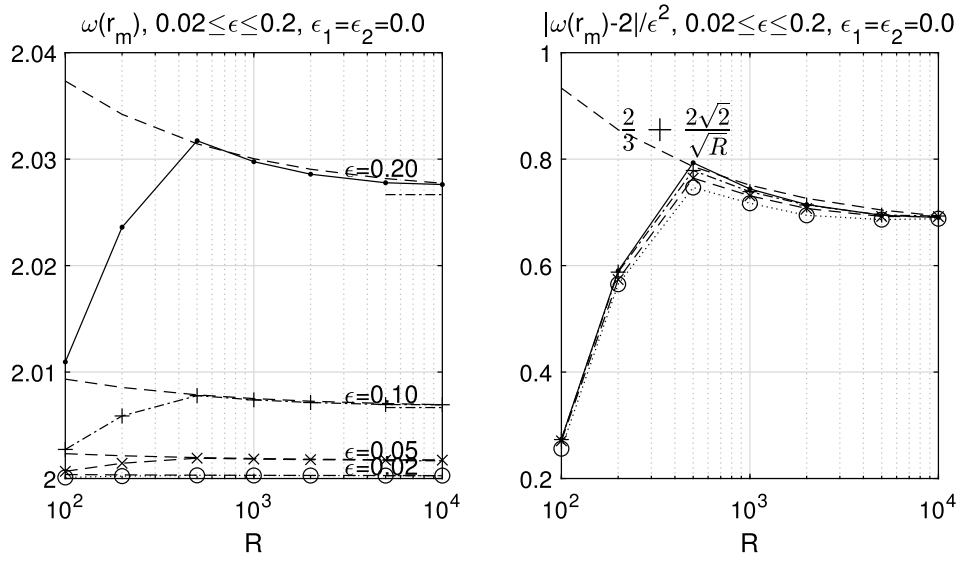

FIG. 6. *Computed vorticity values with asymptotic formula (black dash line) for* $10^2 \le R \le 10^4$ *and* $q_1 = 1/2$, $q_2 = 1 + \epsilon \sin\theta$, $0.02 \le \epsilon \le 0.2$.

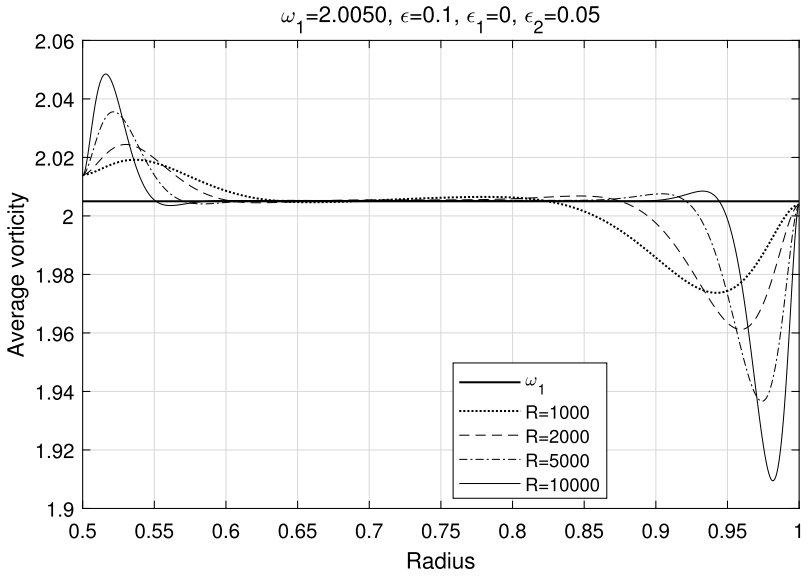

FIG. 7. *Vorticity profiles for* $q_1 = 1/2 + 0.05\cos\theta$, $q_2 = 1 + 0.1\sin\theta$.

a superposition of the two boundary layers. Figure 8 shows the vorticity profile for $(\epsilon, \epsilon_1, \epsilon_2) = (0.1, 0, 0.1)$. As we expect from the preceding cases, there generally appear two boundary layers near the inner and the outer boundary but the perturbation from the inner boundary affects the flow more than that of the outer boundary. The consistency with numerical results confirms the validity of (6.10) for both wall velocity perturbed cases.

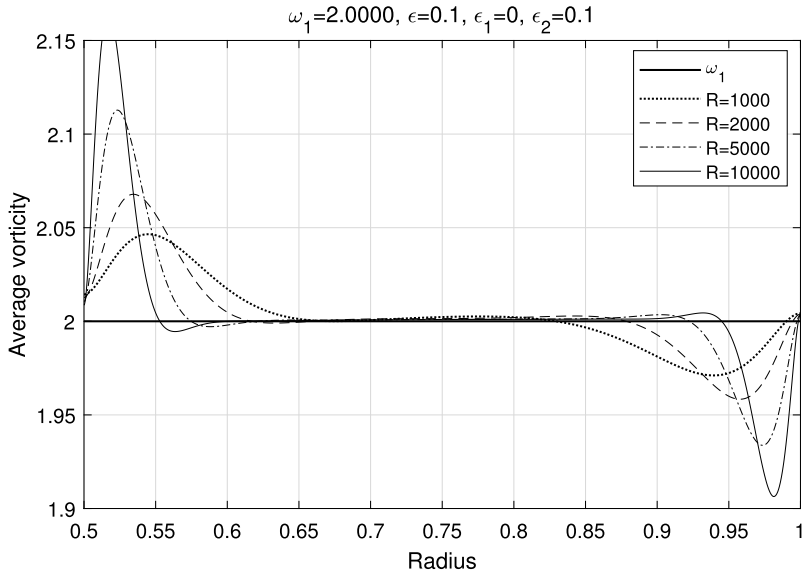

FIG. 8. *Vorticity profiles for* $q_1 = 1/2 + 0.1\cos\theta$, $q_2 = 1 + 0.1\sin\theta$.

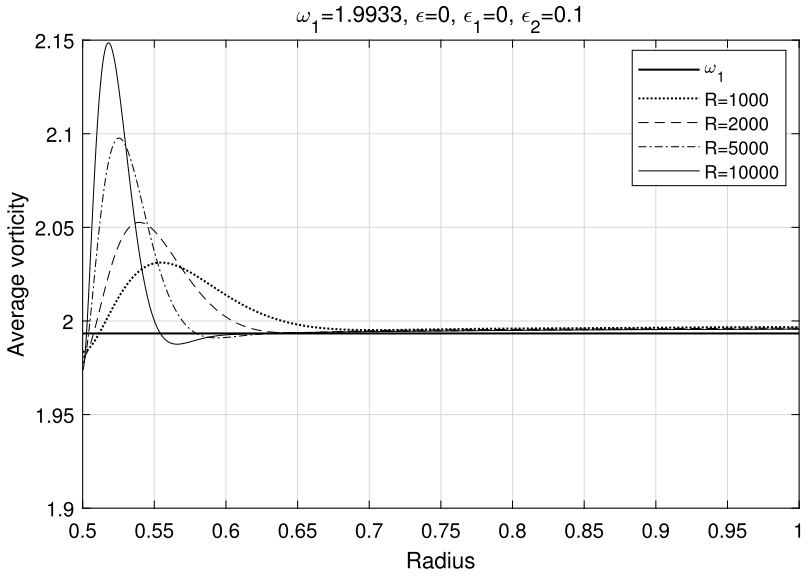

FIG. 9. *Vorticity profiles for* $q_1 = 1/2 + 0.1\cos\theta$, $q_2 = 1$.

Experiment 8 (vorticity profile for stronger inner perturbation).

We finally consider the stronger inner perturbation case and Figure 9 shows the numerical result of the vorticity values for $q_1 = 1/2 + 0.1\cos\theta$, $q_2 = 1$. We notice that the numerical results are slightly increasing for $r > 2/3$ and a rather small but noticeable difference exists between the asymptotic result ω_1 and numerical values around $r = 1$. This phenomenon occurs when $\sqrt{\epsilon_1^2 + \epsilon_2^2}$ is bigger than ϵ in our numerical computation. We do not know the exact reason for this difference but possibly is

due to the stronger effect of the inner perturbation than the outer perturbation. This point is explained in more detail below in section 7.

7. Concluding remark. In this paper, we study the incompressible viscous fluid flow at large Reynolds numbers in an annulus. We properly extend the PB theory to apply to these types of flows. The BW formula for the inviscid limit of vorticity is derived analogously, and a further correction of the second-order result is calculated using a matching technique in the expansion. To validate the theoretical results, we perform suitable numerical computations employing a highly accurate numerical method. In this context, we offer two important observations.

First, the comparison shows good agreement with asymptotic formulas in the case of perturbed outer wall velocity. However, a type of weak layer appears near the unperturbed boundary which possibly shows the discrepancy in the inviscid limit flow. This phenomenon is not physically observable, as the velocity remains continuous while the vorticity is discontinuous. A similar occurrence of continuous velocity and discontinuous vorticity is noted in the counterrotating eddies after an obstacle [17] and viscous shedding of the Sadovskii dipole [7]. However, in those cases, the physical boundary effect is absent. We suppose that it may contribute to inaccuracies in the theoretical predictions.

On the other hand, we observe an increased discrepancy between the theoretical and numerical results for the cases where the inner wall velocity is perturbed or both walls are perturbed. The exact reason for this is unclear; however, we hypothesize that the inner boundary, having double the curvature of the outer boundary, might exert a stronger influence on the flow. (Recall that we assume the unperturbed flow depends only on r suggesting that the inner flow is potentially more affected by the same perturbation than the outer flow.) These two aspects remain only partially understood and warrant further investigation in future research.

For convenience, we restrict our study to the concentric annular domain. There is a clear potential for extending the present results to eccentric annuli or more general multiply connected domains in two dimensions. In such investigations, the first issue to consider is the stability of the flow, as most flows tend to become unstable at large R [10]. Bifurcations possibly occur with increasing R, complicating the identification of a definitive inviscid limit for the flow. In connection to this, we refer to recent work that presents an explicit formula to describe a possible Euler limit flow in general multiply connected domains, using the Schottky–Klein prime function in complex variables. This approach provides a family of conformal mappings that transform such complex domains into standard, simpler canonical domains [8].

Another possible extension to mention is the flow reversal in the boundary layers. We perturb the wall velocity by a relatively small amount so that there is no flow reversal inside the boundary layer. However, the case of larger perturbation can be also discussed for a marginal separation case [19] and further general separation case [25, 31, 33].

Appendix A. Additional calculations on the second order expansion terms.

A.1. Computation of P_1 and P_2. Applying the matching principle to the first two terms of pressure, we have the condition for $p_2(x, Y)$,

$$p_2(x, Y) \sim Y \frac{\partial P_1}{\partial y}(x, 0) + P_2(x, 0) \quad \text{as} \quad Y \to \infty. \tag{A.1}$$

Then, P_1, P_2 are computed in the following manner. Forming the inner product of $\mathbf{U}$ with the first equation in (2.1) gives the kinematic energy equation

$$\mathbf{U}\cdot\nabla\left(P+\frac{1}{2}U^2\right)-R^{-1}\mathbf{U}\cdot\nabla^2\mathbf{U}=0. \tag{A.2}$$

Substituting $\mathbf{U}=(U,V)$ as given in (4.7) into this, the $O(1)$ terms yields

$$P_1+\frac{1}{2}\mathbf{U}_1\cdot\mathbf{U}_1=B_1(\Psi_1). \tag{A.3}$$

Similarly, the $O(1/\sqrt{R})$ terms satisfy

$$P_2+\mathbf{U}_1\cdot\mathbf{U}_2=\Psi_2 B_1{}'(\Psi_1)+B_2(\Psi_1), \tag{A.4}$$

where B_1, B_2 are first and second Bernoulli functions [29].

In our case, we note that $B_1{}'(\Psi_1)=-\Omega_1(\Psi_1)=-\Omega_1(r)$. As we assumed the outer flow is independent of Reynolds number, we may take $B_2=0$. It follows that

$$\frac{\partial P_1}{\partial y}(x,0)=-{U_1}^2(x,0) \tag{A.5}$$

and from (A.4), that

$$P_2(x,0)=\Psi_2(x,0)B_1{}'(0)-U_1(x,0)U_2(x,0). \tag{A.6}$$

We thus obtain the corresponding pressure boundary condition as $Y\to\infty$,

$$p_2(x,Y)=-Y+\left(C_{21}+\sum_{n\neq 0}\frac{c_n}{\sqrt{in}}(|n|-2)e^{inx}\right)\epsilon+O(\epsilon^2). \tag{A.7}$$

A.2. Computation of $(u_2, v_2, p_2)(x, Y; \epsilon)$. The second term of the inner expansions are expanded as

$$(u_2,v_2,p_2,\omega_2)(x,Y;\epsilon)=(u_{20},v_{20},p_{20},\omega_{20})(x,Y)+\epsilon(u_{21},v_{21},p_{21},\omega_{21})(x,Y)+\cdots.$$

We need to compute the first three terms in these expansions.

A.2.1. Computations of $u_{20}(x,Y), v_{20}(x,Y), p_{20}(x,Y), \omega_{20}(x,Y)$. Substituting the expansion into (4.25)–(4.26) and solving O(1) terms, we obtain

$$u_{20}(x,Y)=-Y,\quad v_{20}(x,Y)=0,\quad p_{20}(x,Y)=-Y. \tag{A.8}$$

A.2.2. Computations of $u_{21}(x,Y), v_{21}(x,Y), p_{21}(x,Y), \omega_{21}(x,Y)$. Next collecting $O(\epsilon)$ terms, we have the system

$$\frac{\partial u_{21}}{\partial x}+\frac{\partial v_{21}}{\partial Y}=\frac{\partial}{\partial Y}(v_{11}Y),\ \frac{\partial p_{21}}{\partial Y}=-2u_{11},$$

$$\frac{\partial u_{21}}{\partial x}-v_{11}-Y\frac{\partial u_{11}}{\partial x}=-\frac{\partial p_{21}}{\partial x}+\frac{\partial^2 u_{21}}{\partial Y^2}-\left\{Y\frac{\partial^2 u_{11}}{\partial Y^2}+\frac{\partial u_{11}}{\partial Y}-u_{10}v_{11}\right\}, \tag{A.9}$$

$$u_{21}(x,0)=v_{21}(x,0)=0, \tag{A.10}$$

$$u_{21}(x,\infty)\sim -2B_{21}-C_{21}-\sum_{n\neq 0}c_n\frac{|n|}{\sqrt{in}}e^{inx},$$

$$p_{21}(x,\infty)\sim C_{21}+\sum_{n\neq 0}\frac{c_n}{\sqrt{in}}(|n|-2)e^{inx}.$$

We obtain immediately

$$p_{21}(x,Y) = C_{21} + 2\sum_{n\neq 0}\frac{c_n}{\sqrt{in}}e^{inx-\sqrt{in}Y} + \sum_{n\neq 0}\frac{c_n}{\sqrt{in}}(|n|-2)e^{inx}. \tag{A.11}$$

Inserting this into (A.9), we have

$$u_{21}(x,Y) = \sum_{n\neq 0} c_n\left[\left\{\frac{1}{2}Y + \frac{|n|}{\sqrt{in}}\right\}e^{-\sqrt{in}Y} - \frac{|n|}{\sqrt{in}}\right]e^{inx},$$

$$v_{21}(x,Y) = \sum_{n\neq 0} c_n\left[\left\{\frac{3}{2}\sqrt{in}Y + \left(\frac{1}{2}+|n|\right)\right\}e^{-\sqrt{in}Y}(|n|-1)\sqrt{in}Y - \left(\frac{1}{2}+|n|\right)\right]e^{inx}.$$

A.2.3. Computation of $u_{22}(x,Y), v_{22}(x,Y), p_{22}(x,Y), \omega_{22}(x,Y)$. The next order terms satisfy

$$\begin{aligned}\frac{\partial u_{22}}{\partial x} + \frac{\partial v_{22}}{\partial Y} &= \frac{\partial}{\partial Y}(v_{12}Y), \quad \frac{\partial p_{22}}{\partial Y} = -({u_{11}}^2 + 2u_{10}u_{12})\frac{\partial u_{22}}{\partial x}\\ &+ u_{11}\frac{\partial u_{21}}{\partial x} + v_{11}\frac{\partial u_{21}}{\partial Y} + v_{12}\frac{\partial u_{20}}{\partial Y} + u_{21}\frac{\partial u_{11}}{\partial x} + u_{20}\frac{\partial u_{12}}{\partial x} + v_{21}\frac{\partial u_{11}}{\partial Y}\\ &= -\frac{\partial p_{22}}{\partial x} + \frac{\partial^2 u_{22}}{\partial Y^2} - \left\{Y\left(\frac{\partial^2 u_{12}}{\partial Y^2} - v_{11}\frac{\partial u_{11}}{\partial Y}\right) + \frac{\partial u_{12}}{\partial Y} - u_{11}v_{11} - v_{12}\right\}.\end{aligned} \tag{A.12}$$

The solutions of these are a complicated expression of the sums of the exponentials. Since we need only the vorticity at the outer edge of the boundary layer, we average these equations with respect to x from 0 to 2π (denoted by overbar):

$$\overline{\frac{\partial v_{22}}{\partial Y}} = \frac{\partial}{\partial Y}(\overline{v_{12}}Y), \quad \overline{\frac{\partial p_{22}}{\partial Y}} = -(\overline{u_{11}^2} + 2\overline{u_{10}u_{12}}), \tag{A.13}$$

$$\begin{aligned}\overline{v_{11}\frac{\partial u_{21}}{\partial Y}} + \overline{v_{12}\frac{\partial u_{20}}{\partial Y}} + \overline{u_{20}\frac{\partial u_{12}}{\partial x}} + \overline{v_{21}\frac{\partial u_{11}}{\partial Y}} &= \overline{\frac{\partial^2 u_{22}}{\partial Y^2}}\\ - \left\{Y\left(\overline{\frac{\partial^2 u_{12}}{\partial Y^2}} - \overline{v_{11}\frac{\partial u_{11}}{\partial Y}}\right) + \overline{\frac{\partial u_{12}}{\partial Y}} - \overline{u_{11}v_{11}} - \overline{v_{12}}\right\}&.\end{aligned} \tag{A.14}$$

The corresponding boundary conditions are

$$\overline{u_{22}}(0) = \overline{v_{22}}(0) = 0, \ \overline{u_{22}}(Y) \sim -\frac{1}{2}Y\sum_{n\neq 0}|c_n|^2 - 2B_{22} - C_{22} \tag{A.15}$$

as $Y\to\infty$. The final equation on $\overline{u_{22}}(Y)$ is

$$\begin{aligned}\frac{\partial^2\overline{u_{22}}}{\partial Y^2} = \sum_{n\neq 0}|c_n|^2\Big[&\left\{((2-\sqrt{2})+3)|n|Y + \sqrt{|n|} - (1+2|n|)\sqrt{in}\right)\right\}e^{-\sqrt{2|n|}Y}\\ &+ \left\{\left(\frac{3}{2}-|n|\right)|n|Y - \frac{1}{2}\sqrt{in} + \frac{1}{2}\sqrt{-in} - |n|\sqrt{2|n|}\right\}e^{-\sqrt{-in}Y}\Big].\end{aligned}$$

Integrating twice and using (A.15), we find

$$2B_{22} + C_{22} = -2\sum_{n>0}|c_n|^2\frac{4-n}{\sqrt{2n}}. \tag{A.16}$$

For the case $f(x) = \sin x$, this becomes

$$2B_{22} + C_{22} = -\frac{3\sqrt{2}}{4}. \tag{A.17}$$

REFERENCES

[1] H. Arbabi and I. Mezić, *Prandtl–Batchelor theorem for flows with quasiperiodic time dependence*, J. Fluid Mech., 862 (2018), R1, https://doi.org/10.1017/jfm.2018.998.

[2] G. K. Batchelor, *On steady laminar flow with closed streamlines at large Reynolds number*, J. Fluid Mech., 1 (1956), pp. 177–190, https://doi.org/10.1017/S0022112056000123.

[3] P. J. Blennerhassett, *A three-dimensional analogue of the Prandtl-Batchelor closed streamline theory*, J. Fluid Mech., 93 (1979), pp. 319–324, https://doi.org/10.1017/S0022112079001919.

[4] P. A. Blythe, A. Liakopoulos, and E. Hacuta, *Thermally driven flows at low Prandtl numbers: An extension of the Prandtl-Batchelor theorem*, Internat. J. Engrg. Sci., 33 (1995), pp. 1699–1711, https://doi.org/10.1016/0020-7225(95)00030-2.

[5] A. V. Bunyakin, S. I. Chernyshenko, and G. Y. Stepanov, *High-Reynolds-number Batchelor-model asymptotics of a flow past an aerofoil with a vortex trapped in a cavity*, J. Fluid Mech., 358 (1998), pp. 283–297, https://doi.org/10.1017/S0022112097008203.

[6] S. Childress, M. Landman, and H. Strauss, *Steady motion with helical symmetry at large Reynolds number*, in Topological Fluid Mechanics, Cambridge University Press, Cambridge, 1990, pp. 216–224.

[7] S. Childress, A. D. Gilbert, and P. Valiant, *Eroding dipoles and vorticity growth for Euler flows in $\mathbb{R}^3$: Axisymmetric flow without swirl*, J. Fluid Mech., 805 (2016), pp. 1–30, https://doi.org/10.1017/jfm.2016.573.

[8] D. G. Crowdy, EH. Kropf, C. C. Green, and M. M. S. Nasser, *The Schottky-Klein prime function: A theoretical and computational tool for applications*, IMA J. Appl. Math., 81 (2016), pp. 589–628, https://doi.org/10.1093/imamat/hxw028.

[9] E. Dormy and H. K. Moffatt, *Prandtl–Batchelor flow in a cylindrical domain*, SIAM J. Appl. Math., 84 (2024), pp. 1658–1667, https://doi.org/10.1137/24M1637313.

[10] P. G. Drazin and W. H. Reid, *Hydrodynamic Stability*, 2nd ed., Cambridge University Press, Cambridge, 2004.

[11] T. D. Drivas, S. Iyer, and T. T. Nguyen, *The Feynman-Lagerstrom criterion for boundary layers*, Arch. Ration. Mech. Anal., 248 (2024), 55, https://doi.org/10.1007/s00205-024-01991-z.

[12] M. Fei, C. Gao, and Z. Lin, *Prandtl–Batchelor flows on a disk*, Comm. Math. Phys., 397 (2023), pp. 1103–1161, https://doi.org/10.1007/s00220-022-04520-9.

[13] M. Fei, C. Gao, Z. Lin, and T. Tao, *Prandtl–Batchelor Flows on an annulus*, Adv. Math., 458 (2024), 109994, https://doi.org/10.1016/j.aim.2024.109994.

[14] R. P. Feynman and P. A. Lagerstrom, *Remarks on high Reynolds number flows in finite domains*, in Proceedings of the IX International Congress on Applied Mechanics, International Congress on Applied Mechanics, Brussels, 3 (1956), pp. 342–343.

[15] H. Fujita, H. Moriomoto, and H. Okamoto, *Stability analysis of Navier-Stokes flows in annuli*, Math. Meth. Appl. Sci., 20 (1997), pp. 959–978, https://doi.org/10.1002/(SICI)1099-1476(19970725)20:11%3C959::AID-MMA895%3E3.0.CO;2-D.

[16] E. W. Haddon and N. Riley, *On flows with closed streamlines*, J. Engrg. Math., 19 (1985), pp. 233–246, https://doi.org/10.1007/BF00042536.

[17] J. F. Harper, *On boundary layers in two-dimensional flow with vorticity*, J. Fluid Mech., 17 (1963), pp. 141–153, https://doi.org/10.1017/S0022112063001178.

[18] S.-C. Kim, *On Prandtl–Batchelor theory of a cylindrical eddy: Asymptotic study*, SIAM J. Appl. Math., 58 (1998), pp. 1394–1413, https://doi.org/10.1137/S0036139996303282.

[19] S.-C. Kim, *Batchelor–Wood formula for negative wall velocity*, Phys. Fluids, 11 (1999), pp. 1685–1687, https://doi.org/10.1063/1.870031.

[20] S.-C. Kim and J.-Y. Lee, *A high-order adaptive numerical method for recirculating flows at large Reynolds number*, J. Comput. Appl. Math., 108 (1999), pp. 75–86, https://doi.org/10.1016/S0377-0427(99)00101-6.

[21] S.-C. Kim and H. Okamoto, *Prandtl–Batchelor theory for Kolmogorov flows*, J. Phys. Soc. Japan, 89 (2020), 114401, https://doi.org/10.7566/JPSJ.89.114401.

[22] E. Lewis, *Steady flow between a rotating circular cylinder and fixed square cylinder*, J. Fluid Mech., 95 (1979), pp. 497–513, https://doi.org/10.1017/S0022112079001579.

[23] J. W. McLaurin, *A general coupled equation approach for solving the biharmonic boundary value problem*, SIAM J. Numer. Anal., 11 (1974), pp. 14–33, https://doi.org/10.1137/0711003.
[24] L. Prandtl, 1904 *Über Flüssigkeitsbewegung bei sehr kleiner Reibung*, in Gesammelte Abhandlungen II, Leipzig Verlag von Wilhelm Engelmann, Leipzig, Germany, 1904.
[25] N. Riley, *High Reynolds number flows with closed streamlines*, J. Engrg. Math., 15 (1981), pp. 15–27, https://doi.org/10.1007/BF00039841.
[26] P. G. Saffman and S. Tanveer, *Prandtl-Batchelor flow past a flat plate with a forward-facing flap*, J. Fluid Mech., 143 (1984), pp. 351–365, https://doi.org/10.1017/S0022112084001385.
[27] M. Sandoval and S. Chernyshenko, *Extension of the Prandtl–Batchelor theorem to three-dimensional flows slowly varying in one direction*, J. Fluid Mech., 654 (2010), pp. 351–361, https://doi.org/10.1017/S0022112010001485.
[28] C. Turfus, *Prandtl–Batchelor flow past a flat plate at normal incidence in a channel–inviscid analysis*, J. Fluid Mech., 249 (1993), pp. 59–72, https://doi.org/10.1017/S0022112093001077.
[29] M. Van Dyke, *Higher approximations in boundary-layer theory, Part* I, J. Fluid Mech., 14 (1962), pp. 161–177, https://doi.org/10.1017/S0022112062001147.
[30] M. Van Dyke, *Perturbation Methods in Fluid Mechanics*, Parabolic Press, Stanford, CA, 1975.
[31] M. Vynnycky, *On the uniform vorticity in a high Reynolds number flow*, J. Engrg. Math., 28 (1994), pp. 129–144, https://doi.org/10.1007/BF00127582.
[32] M. Vynnycky, *Concerning closed-streamline flows with discontinuous boundary conditions*, J. Engrg. Math., 33 (1998), pp. 141–156, https://doi.org/10.1023/A:1004204527294.
[33] M. Vynnycky, *Toward an asymptotic description of Prandtl–Batchelor flows with corners*, Phys. Fluids, 34 (2022), 113613, https://doi.org/10.1063/5.0124851.
[34] L. Van Wijngaarden, *Prandtl-Batchelor flows revisited*, Fluid Dyn. Res., 39 (2006), pp. 267–278, https://doi.org/10.1016/j.fluiddyn.2006.07.006.
[35] W. W. Wood, *Boundary layers whose streamlines are closed*, J. Fluid Mech., 2 (1957), pp. 77–87, https://doi.org/10.1017/S0022112057000749.
[36] T. Yamagata and T. Matsuura, *A generalization of Prandtl-Batchelor theorem for planetary fluid flows in a closed geostrophic contour*, J. Meteor. Soc. Japan. Ser. II, 59 (1981), pp. 615–619, https://doi.org/10.2151/jmsj1965.59.5_615.